



## Wheat gliadin hydrolysates based nano-micelles for hydrophobic naringin: Structure characterization, interaction, and in vivo digestion

Zhiyong Wang<sup>a,1</sup>, Xiaoyi Cheng<sup>a,1</sup>, Fanda Meng<sup>a</sup>, Haotong Guo<sup>a</sup>, Zhengqin Liu<sup>a</sup>, Huan Wang<sup>b</sup>, Jing Xu<sup>a,\*</sup>, Hua Jin<sup>a,\*</sup>, Lianzhou Jiang<sup>b</sup>

<sup>a</sup> College of Arts and Sciences, Northeast Agricultural University, Harbin, Heilongjiang 150030, China

<sup>b</sup> College of Food Science, Northeast Agricultural University, Harbin, Heilongjiang 150030, China

### ARTICLE INFO

#### Keywords:

Wheat gliadin  
Enzymolysis  
Micelle  
Naringin  
Delivery

### ABSTRACT

In this study, enzymatic hydrolysis was used to fabricate wheat gliadin hydrolysates (WGHs) for the encapsulation and protection of naringin. The exposure of hydrophilic amino acids decreased the critical micelle concentration (from  $0.53 \pm 0.02$  mg/mL to  $0.35 \pm 0.03$  mg/mL) and improved solubility, which provided amphiphilic conditions for the delivery of naringin. The hydrolysates with a degree of hydrolysis (DH) of 9 % had the strongest binding affinity with naringin, and exhibited the smallest particle size ( $113.7 \pm 1.1$  nm) and the highest encapsulation rate ( $83.2 \pm 1.3$  %). The storage, heat and photochemical stability of naringin were improved via the encapsulation of micelles. Furthermore, the micelles made up of hydrolysates with a DH of 12 % significantly enhanced the bioavailability of naringin (from  $19.4 \pm 4.3$  % to  $46.8 \pm 1.4$  %). Our experiment provides theoretical support for the utilization of delivery systems based on water-insoluble proteins.

### 1. Introduction

Wheat is a crop that is necessary for human survival and has a strong ability to adapt to the environment, making it the most widely grown and productive grain crop in the world (Barak, Mudgil, & Khatkar, 2015). Wheat gliadin (WG) is one of the major storage proteins of wheat, which makes up approximately 30 % of the total protein content. The structure of WG consists of two main regions: a central region rich in glutamine and proline and a terminal region surrounded by hydrophobic amino acids, resulting in the unique amphiphilic property of WG (Qi, Wei, Yue, Yan, & Zheng, 2006). However, the existence of intramolecular disulfide bond and hydrophobic interactions lead to the extremely low solubility of WG in water at neutral pH, and restricts the application in the food industry (Fathi, Donsi, & McClements, 2018).

The modification to protein structures is a common method used to broaden their application range. Physical or chemical treatments have been developed to improve the structural properties of WG. Frozen storage was an efficient method to modified the structure of WG, which reduced the surface hydrophobicity and surface tension, and led to the improvement of the foam stability of WG (Wang et al., 2014). Besides, acetic anhydride modification was also applied to improve the surface

hydrophilicity of WG, which promoted the water solubility, water holding, emulsifying, and foaming properties of WG (Majzoubi, Abedi, Farahnaky, & Aminlari, 2012). Lower modification effects and the use of chemical reagents limit the application of physical or chemical methods in the food industry. One possible efficient approach to improve the functional properties of WG without causing security issues could be controlled enzymatic hydrolysis. Appropriate enzymatic processing has the ability to improve the structure of proteins effectively and steer hydrolysis toward the desired hydrolysis products by controlling reaction conditions. Enzymatic hydrolysis decreases the molecular weight of proteins and increases the accessibility of hydrophobic or hydrophilic regions in the protein structure, which improves the solubility and amphiphathy of proteins.

The application range of protein in the aqueous phase could increase on account in the improvement of solubility. Previous studies have also examined that amphiphilic polypeptides show a trend of self-assembly in water (Tavano, Berenguer-Murcia, Secundo, & Fernandez, 2018). The process of enzymatic hydrolysis develops amphiphilic polypeptides containing hydrophobic and hydrophilic fragments, and spontaneously self-assemble into micelles with core-shell structures in the water medium under the prompting of hydrophobic interactions. The formation

\* Corresponding authors.

E-mail addresses: [xujing@neau.edu.cn](mailto:xujing@neau.edu.cn) (J. Xu), [jinhua@neau.edu.cn](mailto:jinhua@neau.edu.cn) (H. Jin).

<sup>1</sup> Co-first author.

of amphiphilic polypeptides improves the delivery capacity of protein for water-insoluble compounds and constructs nanocarriers with smaller particle size and better stability to resist adverse external conditions and digestive environments (Wang, Wang, Yang, Guo, & Lin, 2015). Lepidium sativum protein hydrolysate produced by pepsin was able to greatly increase the solubility, stability, and bioavailability of curcumin (Kadam, Palamthodi, & Lele, 2019). However, most of the research focused on water-soluble proteins at present, and the delivery property of polypeptides formed by water-insoluble proteins, such as WG was rarely discussed.

Naringin is a natural flavonoid extracted from citrus plants that presents various biological effects, such as anti-inflammatory, antibacterial, antioxidant, and anti-tumor properties. Nevertheless, its application in the food industry is restricted due to low water solubility and environmental sensitivity, leading to bad bioavailability during the digesting process (Ruthvika, Yogesh, & Sarika, 2018). A promising strategy to overcome these limitations involves encapsulating naringin within a nanocarrier delivery system.

Enzymatic hydrolysis destroyed the structure of WG, and amphiphilic polypeptides were generated, which can be applied to encapsulate hydrophobic active substances. In this study, peptides with different DHs were obtained by controlling hydrolysis time. The effect of enzymatic hydrolysis on the structure and amphiphilicity of WG was studied. And the self-assembly method was applied to form nano-micelles loaded with naringin. The strength of the interaction force and the morphology of micelles were investigated, as well as the storage and photothermal stability. Additionally, the *in vitro* digest behavior of micelles loaded naringin was evaluated. This research demonstrates the great potential of water-insoluble proteins to encapsulate and protect hydrophobic bioactive substance in food and pharmaceutical applications.

## 2. Material and methods

### 2.1. Materials

Gluten was purchased from Baiting Food Co., Ltd (Shandong, China). Naringin (Macklin, 97 % purity). Alcalase (activity 200 U/mg) was purchased from Yuanye Biotechnology Co., Ltd (Shanghai, China). All other chemical reagents obtained were of analytical grade.

### 2.2. Protein extraction

WG was extracted from gluten according to a described procedure previously (Peng et al., 2017). Briefly, the gluten was defatted twice by dichloromethane, and then blended with 70 % ethanol at a ratio of 1:10 (w/v) for 3 h. Supernatant was centrifuged at 8000 g for 10 min, and ethanol was removed by a rotary evaporation instrument (R-300, Buchi, Switzerland) at 40 °C. WG was separated from the liquid phase by freeze-drying. The protein content (89.0 ± 0.3 %) was analyzed by a nitrogen analyzer (NDA 702, VELP Scientifica, Italy).

### 2.3. Preparation and characterization of wheat gliadin hydrolysates

#### 2.3.1. Enzymatic hydrolysis of WG

WG was dispersed into deionized (1 %, w/v), stirred for 20 min at 55 °C, and adjusted pH to 8.5. Alcalase was mixed with solution (enzyme to substrate ratio was 0.03), and added 0.5 M NaOH continuously during hydrolysis to maintain the pH. In order to terminate the reaction, the obtained solution had to be heated at 95 °C for 5 min to inactivate the enzyme, and centrifuged to get the supernatant. The final solution was freeze-dried to obtain wheat gliadin hydrolysates (WGH). The hydrolysates formed with 3 %, 6 %, 9 %, 12 % and 15 % degree of hydrolysis (DH) were named as WGH-3, WGH-6, WGH-9, WGH-12 and WGH-15, respectively. DH was calculated according to the following equation:

$$\text{DH} (\%) = \frac{B \times N_b}{\alpha \times M \times h_{\text{tot}}} \times 100 \quad (1)$$

where  $B$  refers to the consumption of base (mL);  $N_b$  is the base concentration (0.5 M);  $M$  is the mass of WG (g);  $\alpha$  represents the average degree of dissociation of  $\alpha$ -amino groups;  $h_{\text{tot}}$  is the total peptide bonds in protein (8.38 meq/g protein).

#### 2.3.2. Sodium dodecyl sulfate–polyacrylamide gel electrophoresis (SDS-PAGE)

SDS-PAGE experiment of WG and WGHs were operated according to previous method (Avramenko, Low, & Nickerson, 2013). 30  $\mu\text{L}$  Samples (8 mg/mL) were mixed with 10  $\mu\text{L}$  sample buffer containing 5 %  $\beta$ -mercaptoethanol, and heated at 100 °C for 5 min. 10  $\mu\text{L}$  of each sample was injected into the gels composed of 4 % stacking gel and 16 % separating gel) for electrophoresis. Coomassie brilliant blue and methanol solutions were used as dyeing agents and decolorizing agents, respectively. A gel imager (Tanon-1600, Shanghai, China) was used to take an image of the gel after detaining it for 24 h. A broad range molecular weight standard marker was used to determine apparent molecular weights (Solabel Technology Co., Ltd., Beijing, China).

#### 2.3.3. Dynamic light scattering (DLS)

The colloidal properties of protein samples were determined by the Malvern Zetasizer (Nano-ZS90, Malvern Instruments Co., Ltd., UK) at 25 °C. The sample concentration was adjusted to 0.1 mg/mL to avoid multiple scattering effects. Each measurement was repeated 3 times under the same conditions (Cheng et al., 2023).

#### 2.3.4. Turbidity

The turbidity was determined by measuring the absorbance of the hydrolysates at 600 nm with an ultraviolet spectrophotometer (UV 2550, Shimadzu Corporation, Tokyo, Japan). Each sample was tested three times.

#### 2.3.5. Fourier transform infrared spectroscopy (FT-IR)

Potassium bromide (KBr) tableting method is often used to determine the FT-IR spectra of different samples. Briefly, 1.0 mg of freeze-dried samples were mixed with 98 mg pure KBr, and scanned with a Fourier transform infrared spectrometer (IRTrace-100, Shimadzu Corporation, Tokyo, Japan). All the samples spectrum was collected over the wavenumber range of 4000–400  $\text{cm}^{-1}$ , and KBr tablet was used as baseline.

#### 2.3.6. Circular dichroism (CD)

The far ultraviolet spectrogram of WG and WGHs were analyzed using a circular dichroism spectrometer (Chirascan, Applied Photo-physics Leatherhead, UK). The concentration of the sample solutions was adjusted to 0.1 mg/mL according to test experiment. The solutions were added into a 100  $\mu\text{L}$  quartz container with a 0.1 cm path length, and scanned the spectrum of samples from 190 to 260 nm in a nitrogen environment. The secondary structure content of samples was obtained by analyzing the spectrum through CD Pro software.

#### 2.3.7. Critical micelle concentration (CMC)

CMC was determined by pyrene fluorescence probe spectrometry (Wu, Zhao, Huang, Ye, & Zhao, 2020). A pyrene solution was prepared as a reserve solution with a concentration of  $1 \times 10^{-6}$  M. 200  $\mu\text{L}$  of pyrene was stored in a test tube, and ethanol was removed. 2 mL of different concentrations of sample solutions (0.001, 0.005, 0.01, 0.05, 0.1, 0.5, 1, 1.5, 2, 2.5 mg/mL) was added, and sonicated for 10 min. The fluorescence spectra of pyrene were recorded from 350 nm to 500 nm using a fluorescence spectrophotometer (FL 4700, Hitachi High-Technologies Corp., Tokyo, Japan), which set the excitation wavelength at 335 nm and the slit width of emission and excitation at both 5

nm. The CMC value was obtained after fitting the log plots of  $I_1/I_3$  and the log concentration of WGHs.

### 2.3.8. Surface hydrophobicity ( $H_0$ )

As an external fluorescence probe, 1-anilino-8-naphthalene sulpho-nate (ANS) often used to determine the surface hydrophobicity ( $H_0$ ) of different protein samples. Different samples were diluted ranging from 0.1 to 0.5 mg/mL using phosphate buffer (10 mM, pH 7.0). The mixture composed of 20  $\mu$ L of ANS solution (8 mmol/L) and 4 mL of the diluted sample solution was incubated away from light at ambient temperature. The fluorescence intensity of the samples was measured by using a fluorescence spectrophotometer (FL 4700, Hitachi High-Technologies Corp., Tokyo, Japan), and excitation and emission wavelengths were set to 390 and 470 nm, respectively.  $H_0$  was considered as the slope of fluorescence intensity to protein concentration.

### 2.3.9. Protein solubility

Protein solubility was analyzed using the Lowry method with slightly modification. The pH of sample solutions (0.1 %, w/v) was adjusted 7. Insoluble substance was removed from solution by centrifuging at 4800 g for 15 min, and bovine serum albumin as standard. Solubility of samples was expressed as the ratio of the protein content in the supernatant to the total protein content measuring by nitrogen analyzer.

## 2.4. Preparation and characterization of WGH-Naringin complex micelles

### 2.4.1. Preparation of WGH-naringin complex micelles

WGHs were dissolved in ultrapure water and gave a final concentration of 5 mg/mL. Stock solution of naringin (2 mg/mL in ethanol) was prepared before experiment. The stock solution and WGHs were mixed at a volume ratio of 1:12, and stirred for 4 h protected from light. Then the mixture was centrifuged at 8,000 g, 4 °C for 10 min. The ethanol was removed by dialysis (1000 Da) overnight, and lyophilized for later use. The sample prepared by using different DHs of protein were named as M(Nar)-3, M(Nar)-6, M(Nar)-9, M(Nar)-12, M(Nar)-15, respectively.

### 2.4.2. The encapsulation efficiency (EE) of naringin

High-performance liquid chromatography (HPLC) system (U3000, Thermo Fisher Scientific, America) was used to quantify the naringin content of samples. 10 mL of methanol was added to the test tube to dissolve the unencapsulated naringin. The mixture was sonicated for 10 min and centrifugated. The resulting supernatant was collected and the volume was adjusted to 10 mL. The experimental method was modified according to the pervious method (Chaaban, Ioannou, Paris, Charbonnel, & Ghoul, 2017). The chromatographic column was an Acclaim PolarAdvantage II column (250  $\times$  4.6 mm, 5  $\mu$ m). The detection wavelength was 288 nm and the injected solution was 20  $\mu$ L. The mobile phase was phase A (40 % ultrapure water) and phase B (60 % methanol), freshly prepared and sonicated before use, and the flow rate was set at 1.0 mL/min. The gradient elution program was proceeded according to pervious method: 95 % (A) at time 0 up to 100 % (B) at 10 min and finally 95 % (A) at 20 min before the end of the program. The encapsulation efficiency (EE) was derived from the following equation:

$$EE(\%) = \frac{\text{Total amount of naringin} - \text{free amount of naringin}}{\text{Total amount of naringin}} \times 100 \quad (2)$$

### 2.4.3. Steady-state fluorescence spectra

The fluorescence intensity of complex micelles was measured by fluorometer to investigate the complexation between WGH and naringin. The concentration of hydrolysates was kept at 0.1 mg/mL, and naringin solution (0, 0.25, 0.5, 0.75, 1.0, 1.25 mg/mL) was added continuously through a syringe. Fluorescence spectra of all the samples were acquired from emission recorded from 300 to 400 nm, and excited at 280 nm. The fluorescence intensity of sodium phosphate buffer was removed as background. The excitation and emission slit widths used

were both 5 nm. Stern-Volmer quenching constant  $K_{sv}$  was calculated according to the following equation (Zhang, Xie, Feng, Liu, & Luo, 2021):

$$\frac{F_0}{F} = 1 + K_{sv}[Q] = 1 + K_q\tau_0[Q] \quad (3)$$

$$\lg\left(\frac{F_0 - F}{F_0}\right) = \lg K_b + n\lg[Q] \quad (4)$$

where  $F_0$  and  $F$  mean the fluorescence intensity of WGHs without or with quencher (naringin),  $Q$  is the concentration of naringin,  $K_q$  is the quenching rate constant,  $\tau_0$  is the average fluorescence lifetime of bio-macromolecules without naringin ( $10^{-8}$  s).  $K_b$  represents the binding constant and  $n$  is the number of binding sites.

### 2.4.4. Transmission electron microscopy (TEM)

Transmission electron microscopy (HT 7800, Hitachi High-Technologies Corp., Tokyo, Japan) was adopt to observe the morphology of WGH-Naringin complex micelles. The freshly prepared sample was diluted 50 times before using. The sample was prepared on the carbon coated copper grid, and the sample was stained with 1 % (w/v) phosphotungstic acid.

### 2.4.5. Storage, heat and photochemical stability

All the samples were kept at 25 °C for up to 12 d, and the particle size of samples was determined every 3 d. Free naringin and micelles were directly exposed to a UV lamp for 0–48 h and micelles were also heated at 130 °C for 180 min. The residual rate of naringin was measured by high performance liquid chromatography.

### 2.4.6. In vitro digestion

The model of in vitro digestion was constructed according to the previous method with some modification (Cheng et al., 2024). In short, the artificial gastric juice (30 mL) was mixed with the sample in equal volume, and continuously stirred at 37 °C for 2 h to simulate digestion in the stomach after adjusting the pH to 2.5. After gastric digestion, the obtained sample (30 mL) was stirred with the prepared bile salt solution (30 mL), and the pH of the mixture was adjusted to 7.0. The whole process took about 4 h.

The bioavailability and stability of naringin were figured by centrifugation (15,000 g, 30 min) of small intestine digestion and collection of intermediate micelles. The bioavailability and stability of naringin were calculated by the following formula:

$$\text{Bioavailability}(\%) = \frac{C_3}{C_1} \times 100 \quad (5)$$

$$\text{Stability}(\%) = \frac{C_1}{C_2} \times 100 \quad (6)$$

Where  $C_1$  represents the naringin content after gastrointestinal digestion,  $C_2$  represents the initial naringin content, and  $C_3$  represents r naringin content after centrifugation in micellar phase.

## 2.5. Statistical analysis

All experiments were carried out at least three times, and the results were expressed as means  $\pm$  standard deviations. The statistical data were calculated using SPSS software (version 23.0), and a one-way analysis of variance was performed. P value of statistical data with Duncan test under 0.05 was regarded as statistically significant.

### 3. Results and discussion

#### 3.1. The structural properties of WG and WGHs

##### 3.1.1. Sodium dodecyl sulfate–polyacrylamide gel electrophoresis (SDS-PAGE)

SDS-PAGE image of protein samples under reducing conditions was observed to investigate the molecular weight changes of WG (Fig. 1A). The molecular weight of the original WG was concentrated in 31–43 kDa (Fathi, Donsi, & McClements, 2018). Upon the increase of DH, the bands at 31–43 kDa disappeared accompanied by high intensity of low-molecular-weight bands. When the hydrolysis process reached the middle or final stages, more and more proteins were broken down into peptides below 14.4 kDa. These results implied that the structure of WG changed with the treatment of alcalase. Alcalase could degrade high molecular weight polymers into low molecular weight polypeptides by cutting peptide bonds in proteins, thus affecting the structure of proteins. A similar decline in molecular weight with limited enzymatic hydrolysis has been previously reported for oat protein isolate (Jiang et al., 2015).

##### 3.1.2. Circular dichroism (CD)

CD spectra have been widely used in spectral studies of protein structures, which are sensitive to conformational changes at the molecular level, especially for secondary structure. CD analysis was performed in the far-ultraviolet region of 190–260 nm to get a better understanding of the secondary structure of WG and its hydrolysates. WG showed a maximum negative peak around 207 nm, which was a typical feature of the  $\alpha$ -helix-rich structure, and the peak at 220–230 nm represented a random coil structure, which indicated that WG had an ordered structure (Wu et al., 2020). While increasing DH, the acquired CD spectra showed a shift to a lower wavelength, indicating the dense sphere structure of WG was undermined. The calculated results showed in Fig. 1C suggested that the content of  $\alpha$ -helix decreased from 21.1 % to 5.3 % through continuous hydrolysis to DH 15 %. On the contrary, random coil contents increased from 28.6 % to 41.4 %. This proved that the protein structure was unfolded during enzymatic hydrolysis, which resulted in the orderly  $\alpha$ -helix structures being disrupted and transformed into more flexible and extended random structures. Moreover,

the  $\beta$ -turn comprised predominantly hydrophilic amino acids, and its increased content indicated a more hydrophilic state of the system.  $\beta$ -Sheets are composed of hydrophobic blocks within the protein chain that interact through hydrogen bonding and hydrophobic effects (Yan et al., 2024). Enzymatic hydrolysis notably decreased the  $\beta$ -sheets content from 31.7 % to 24.2 %, signifying a decrease in the hydrophobicity of WGHs. In brief, the hydrolysis of WG is a process that disrupts the intermolecular interactions of proteins, ultimately leading to the destruction of structure and changes in secondary structures, which are more pronounced with increased DH. Furthermore, changes in the content of the secondary structure could impact the hydrophilicity and result in the emergence of additional functional properties.

##### 3.1.3. Fourier-transform infrared spectroscopy (FT-IR)

FT-IR is a common method for analyzing changes in protein during the hydrolysis progress. The FT-IR spectra of hydrolysates obtained at different DHs were similar to the original protein spectrum, which did not display new infrared absorption but with different intensity as shown in Fig. 1E. The broad peak of WG in 3200–3400  $\text{cm}^{-1}$  corresponded to the stretching vibration of O–H. The intensity of WG was higher than that of hydrolysate in this region and decreased gradually with the increase of DH. This change may result from the destruction of hydrogen bonds of hydroxyl (O–H), which reduced the density and strength of hydrogen bonds (Ai et al., 2019). Meanwhile, the absorption peaks in the range of 2800–3000  $\text{cm}^{-1}$  mainly result from the stretching vibrations of C–H bonds, which characterize the change of the hydrophobic interaction of proteins. Compared with the spectra of WG, WGHs shifted to lower wavenumbers, which indicated that enzymatic hydrolysis changed the polar environment of the protein and weakened the hydrophobic interaction. The absorption peaks around 560  $\text{cm}^{-1}$  are the tensile vibrations of S–S bonds (Stefanovic et al., 2018). The intensity of characteristic peaks gradually decreased with the increase of DH, which indicated the decrease in disulfide bond content. The results of FT-IR showed that enzymatic hydrolysis disrupted the hydrogen bonds, hydrophobic interaction, and S–S bonds of WG, which were the main forces that maintained the structural stability of proteins, and led to a conformational transition.

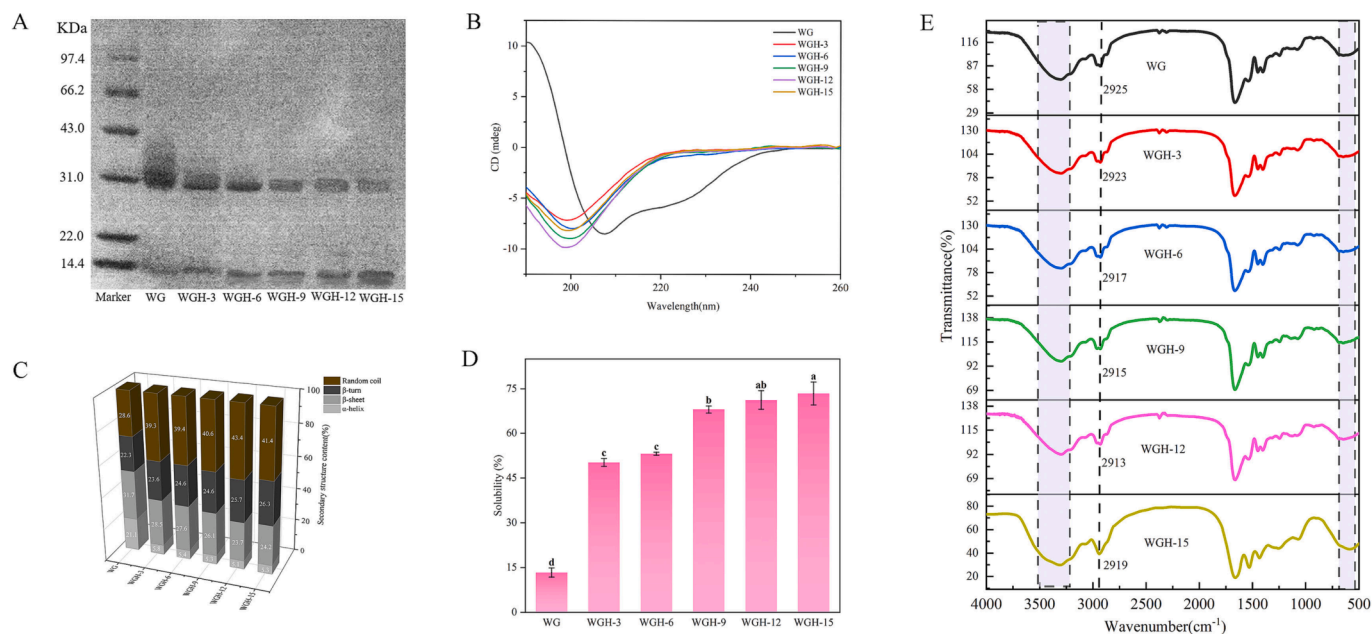


**Fig. 1.** (A) SDS-PAGE profile; (B) Circular dichroism spectra; (C) Second structure contents; (D) Solubility; (E) FTIR spectra of WG and WGHs with different DHs. Different capital letters (a-g) indicate significant difference ( $P < 0.05$ ).

### 3.1.4. Solubility

Solubility is closely related to the structure of protein and is one of the primary prerequisites to ensure the wide application of protein in the food industry. The poor solubility of WG, which was 7.3 % at pH 7, could be put down to a rigid macromolecular structure maintained by intramolecular disulfide bond. Enzymatic hydrolysis of proteins with alcalase significantly improved their solubility in water as shown in Fig. 1D. Enzymatic hydrolysis diminished the molecular weight of protein and unfolded the peptide chain gradually. The number of ionizable amino and carboxyl groups increased, thereby improving the electrostatic repulsion between peptides and preventing their aggregation (Gómez, Gay, Tironi, & Avanza, 2021). This also explains the decrease in turbidity. Smaller peptides generated with higher DH had more polar amino acid residues, which can enhance the bonding with hydrogen bonds in water. Besides, the low solubility of WG in water is the result of synergistic interactions of disulfide bonds and hydrophobic force, which caused the peptide chains to fold and became unable to stretch in an aqueous solution. The destruction of acting force also contributed to cutting the interactions within WG, which may lead to an improvement in protein solubility. Increased solubility may also improve the stability of WGHs in aqueous environments and enhanced their dispersion.

### 3.1.5. Particle size and zeta-potential

Particle size is often used to indirectly reflect the change in protein structure (Table 1). The particle size of WG exceeded 3500 nm, and was dispersed unevenly. This may be due to its extremely low solubility and a tendency to cluster in water. Compared to WG, WGHs with different DHs exhibited smaller particle sizes and were all under 200 nm. WGH-9 showed the minimum particle size. The polypeptide chains were cut smaller with the increase of DH, leading to a decrease in particle size and PDI. However, prolonged heating during the hydrolysis process results in the aggregation of WGHs, thereby increasing the particle size and reducing its dispersion. The value of zeta-potential reflects the magnitude of charge repulsion between charged particles and is an important tool to evaluate the stability of the system. The zeta-potential of WG and its hydrolysates were strongly negative, owing to the fact that the experiment pH was higher than the isoelectric point of WG. The increase of negative charge may be caused by the exposure of negatively charged amino acid after enzymatic hydrolysis. In addition, the increase of

surface charges can strengthen electrostatic repulsion between peptides, making them disperse uniformly. Excessive hydrolysis promoted the aggregation of peptide chains and diminished the content of surface charge.

### 3.1.6. Turbidity

Turbidity is often used to investigate the dispersion of molecules in solution, and is related to the variation of particle size. As illustrated in Fig. 2A, the turbidity of WG was 0.82, which may be on account of its poor solubility in water. The turbidity of hydrolysates was reduced with hydrolysis, and the lowest turbidity value (0.22) was noticed at WGH-12, which was an implication of less formation of aggregates in water. The low turbidity also indicated that the formation of small peptides weakened the light scattering, which was consistent with the data from the particle size determination. However, after a long time of enzymatic hydrolysis with heating, the polypeptides formed a large aggregate via hydrophobic interaction under the drive of heat induction, thus increasing the turbidity.

### 3.1.7. Surface hydrophobicity ( $H_0$ )

Surface hydrophobicity symbolizes the content of hydrophobic amino acids distributed on the protein surface, and can also indirectly represent the change of structure. Besides, surface hydrophobicity also has a great influence on the interactions between proteins. Therefore, the  $H_0$  value of WG and WGHs were quantified by the fluorescent probe method. The surface hydrophobic index of the original protein was 183.58 as shown in Fig. 2B, which may be due to the high content of hydrophobic groups dispersed on the surface of WG. The surface hydrophobicity of WG gradually decreased as the hydrolysis proceeded, indicating that the binding sites of fluorescent probe decreased. The lowest  $H_0$  was obtained for the WGH sample with 9 % DH which was 90.32, and then  $H_0$  increased upon further hydrolysis. The decrease in hydrophobicity may be due to the disruption of internal force within proteins during enzymatic reactions, leading to the exposure of hydrophilic fractions (Jin, Okagu, Yagoub, & Udenigwe, 2021). However, long-term hydrolysis could also result in the aggregation of polypeptides, which influenced the hydrophobic patches on the surface accessible for the ANS probe. Surface hydrophobicity is determined by the size, shape, amino acid composition, and sequence of the protein molecule. WG has a compact, three-dimensional spherical shape and its surface region is mainly comprised of nonpolar amino acids, leading to a high level of hydrophobicity. However, heat treatment and enzymatic process would expose the central regions rich in glutamine and proline, resulting in a reduction in surface hydrophobicity. Furthermore, the formation of  $\beta$ -sheet structure is more likely in a hydrophobic environment. The presence of hydrophilic amino acid residues results in an increase of water in the space between the unfolded molecules, and diminished the  $\beta$ -folding content (Sheng et al., 2020). These findings aligned with the CD analysis.

### 3.1.8. Critical micelle concentration (CMC)

The transition process of amphiphilic copolymers from monomers to aggregates is mainly determined by the critical micelle concentration (CMC) and has a decisive effect on the self-assembled microstructure. The effect of DH on CMC and the corresponding self-assembly behavior of reactants in an aqueous solution were studied by the pyrene fluorescence probe method. The fluorescence spectrum of pyrene usually presents five intensity peaks, where the  $I_1/I_3$  ratio depends on the microenvironment polarity. The  $\pi-\pi^*$  vibration of pyrene in polar media causes an obvious increase in the intensity of  $I_1$ , while  $I_3$  is insensitive to polarity. Thus, when conjugated concentrations exceed CMC to form aggregates, pyrene molecules are immediately captured by their hydrophobic waters, resulting in a sudden decrease in  $I_1/I_3$  (Rajib & Ranjini, 2013). Fig. 2C demonstrated the relationship between the ratio of  $I_1/I_3$  and concentration at different DHs. Pyrene molecules were dispersed in the hydrophilic microdomain of the solution at low

**Table 1**  
Colloidal properties of WGHs and micelles.

	Sample	Particle size (nm)	PDI	Z-potential (mV)	EE (%)
Individual protein	WGH-3	168.30 ± 7.96 <sup>a</sup>	0.388 ± 0.067 <sup>ab</sup>	-21.46 ± 2.02 <sup>a</sup>	N/A
	WGH-6	155.23 ± 3.20 <sup>a</sup>	0.346 ± 0.038 <sup>b</sup>	-27.29 ± 0.23 <sup>b</sup>	
	WGH-9	119.16 ± 6.05 <sup>a</sup>	0.354 ± 0.034 <sup>b</sup>	-28.53 ± 1.43 <sup>b</sup>	
	WGH-12	120.13 ± 6.50 <sup>a</sup>	0.393 ± 0.025 <sup>ab</sup>	-30.33 ± 3.72 <sup>c</sup>	
	WGH-15	149.16 ± 6.04 <sup>a</sup>	0.475 ± 0.097 <sup>a</sup>	-30.01 ± 1.76 <sup>c</sup>	
WGH-naringin complex micelles	M (Nar)-3	132.43 ± 5.33 <sup>B</sup>	0.398 ± 0.017 <sup>A</sup>	-28.95 ± 2.84 <sup>A</sup>	67.72 ± 0.25 <sup>D</sup>
	M (Nar)-6	131.90 ± 1.63 <sup>B</sup>	0.322 ± 0.021 <sup>B</sup>	-30.55 ± 1.70 <sup>A</sup>	74.69 ± 0.59 <sup>C</sup>
	M (Nar)-9	113.70 ± 1.14 <sup>BC</sup>	0.345 ± 0.042 <sup>AB</sup>	-31.93 ± 1.20 <sup>A</sup>	83.18 ± 0.56 <sup>A</sup>
	M (Nar)-12	110.13 ± 9.69 <sup>C</sup>	0.376 ± 0.044 <sup>AB</sup>	-31.04 ± 1.56 <sup>A</sup>	78.97 ± 0.88 <sup>C</sup>
	M (Nar)-15	152.70 ± 7.33 <sup>A</sup>	0.402 ± 0.105 <sup>A</sup>	-30.71 ± 1.51 <sup>A</sup>	74.72 ± 0.59 <sup>C</sup>

Different capital letters (a-c and A-D) indicate a significant difference ( $P < 0.05$ ).

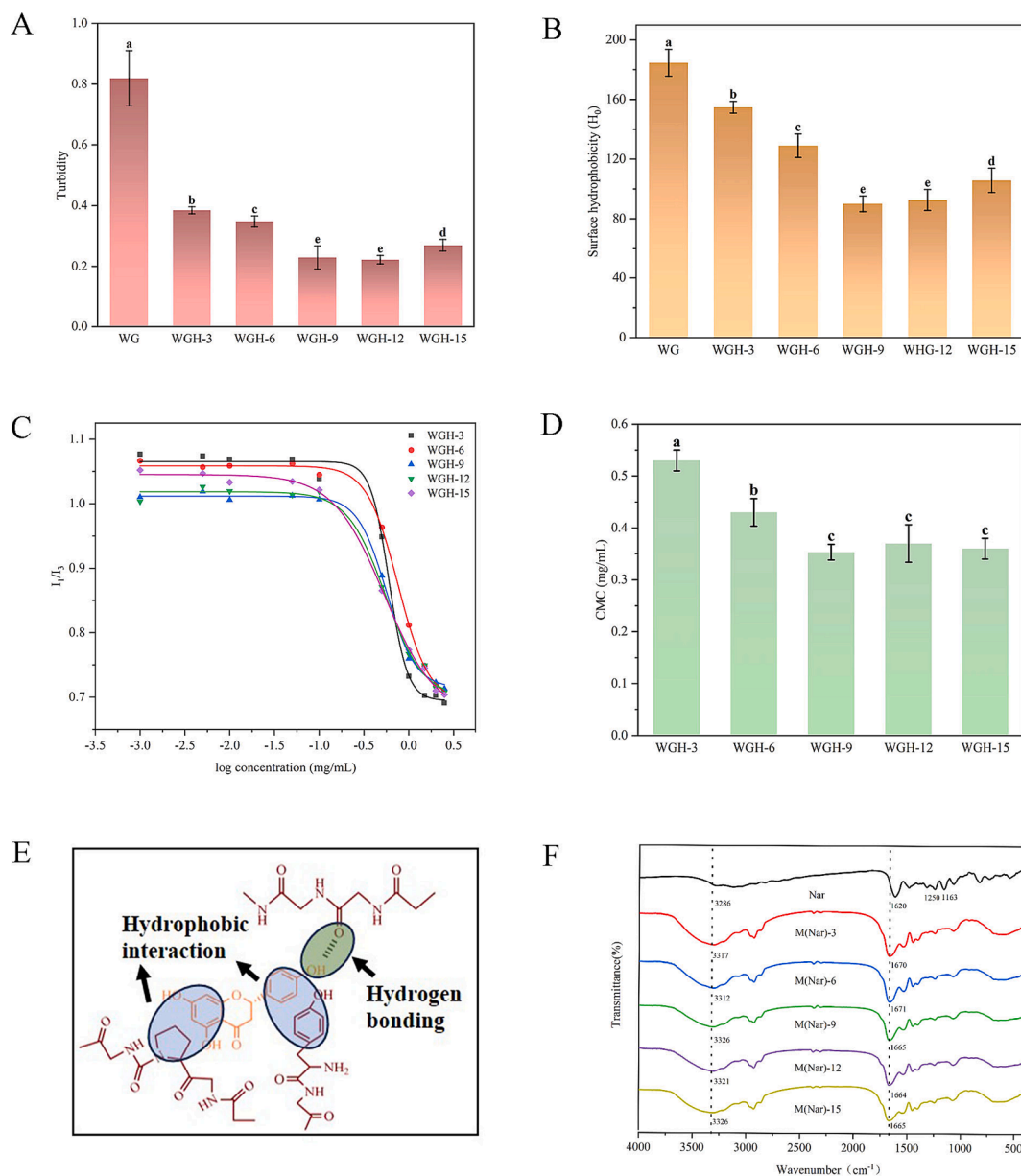


**Fig. 2.** (A) Turbidity; (B) Surface hydrophobic; (C) Fitting curve; (D) CMC value of WG and WGHs with different DH; (E) The interaction mechanisms between naringin and WGHs; (F) FT-IR of WGH-Naringin micelles. Different capital letters (a-e) indicate significant differences ( $P < 0.05$ ).

concentrations, resulting in a higher  $I_1/I_3$  ratio. In contrast, when the concentration exceeded its CMC, the ratio of  $I_1/I_3$  showed a significant decrease due to the movement of pyrene from the polar to the non-polar microenvironment, indicating the formation of aggregates. The value of CMC was showed in Fig. 2D, and showed a trend of first decreasing and then increasing. The change of CMC is mainly affected by two aspects. First, the hydrolysis destroyed the internal force of protein, hydrophilic groups were exposed and weakened the hydrophobic interaction between hydrolysate, resulting in the reduction of CMC. Secondly, long-term heating also destroyed the structure of the external water environment of the aggregates, and the hydrogen bond was not conducive to maintain and stabilize the self-assembled structure, resulting in the increase of CMC. The first reason was more important for hydrolysates, suggesting that exposure to hydrophilic regions, as well as hydrophobic interactions, were critical to the formation of aggregates. Therefore, we believed that the formation and structure transformation of micelle were determined by the balance of hydrophobic and hydrogen bond interactions (Wu et al., 2019). The results of surface hydrophobicity and

particle size combined with the slightly increase of CMC at the high DH stage (DH > 12 %) indicated that peptide aggregation occurred and weakened the amphiphilicity of hydrolysate, which was not enough to form an ordered microparticle structure.

### 3.2. Characterization of WGH-Naringin complex micelles

#### 3.2.1. Colloidal properties of WGH-Naringin complex micelles

The particle size, PDI, and zeta-potential of WGH-Naringin complex micelles were measured to investigate the colloidal properties, as shown in Table 1. Compared with the WGHs, the particle size of the complex with naringin was reduced, which indicated that the more compact structures were generated as a result of the complexation with naringin. A similar conclusion has also been observed in zein hydrolysate complexes. The addition of curcumin caused a decline in particle size (Du et al., 2019). The trend of PDI was similar to that of particle size. The PDI of all samples was less than 0.4, except M(Nar)-15, showing the good dispersion of samples. As described in Table 1, all the micelles had

negative charges, which kept the particles separated and prevented their aggregation. The further increase in the absolute value of the potential may be due to the fact that the finite charge was distributed over a shrunken surface area (Wang, Wang, Guo, Wan, & Yang, 2017).

The encapsulation ability of WGHs micelles was also determined. WGHs may have a greater capacity for loading naringin than WG, which due to that the protein transitioning from a granular to an amphiphilic chain structure, and exhibited more effective capacity in capturing and interacting with naringin. The immense surface hydrophobicity of WG caused its aggregation in water with poor dispersion, thus hindering the effective encapsulation of naringin. Proteolysis resulted in the formation of amphiphilic peptides, which increased the chance to bind with naringin. Additionally, the enhanced solubility also led to stronger hydrogen bonding of the hydrophilic end to the aqueous environment, and generated the formation of a more stable and dispersible micelle structure. The ability of hydrolysates to delivery naringin was restricted, and reached a maximum value of 83.2 % at DH of 9 %. The interaction pattern of naringin with WGHs as described in Fig. 2E. The hydroxyl group (–OH) on the naringin structure was hydrogen donors, and can form hydrogen bonds by interacting with the –OH or amino group on the amino acid side chains. In addition, the hydrophobic amino acids on polypeptide chains, such as proline and phenylalanine residues could interact with the non-polar aromatic ring of naringin (Liu, Zha, Li, Pan, & Luo, 2021). The aggregation and folding of peptides during the extensive hydrolysis process may cause the reaction site to be buried, resulting in a decrease in EE. All the above conclusions indicate that WGHs had certain complexing capacity for naringin, and hydrolysate (DH  $\geq$  9 %) presented better colloidal properties and encapsulation capacity.

### 3.2.2. FT-IR

The FT-IR spectra of naringin and WGH-Naringin micelles were illustrated in Fig. 2F. The characteristic bands of pure naringin were presented at  $3327\text{ cm}^{-1}$  (O–H stretching),  $1620\text{ cm}^{-1}$  (C=O stretching on pyranone),  $1522$  and  $1485\text{ cm}^{-1}$  (C=C on the benzene ring),  $1250$

and  $1191\text{ cm}^{-1}$  (Ar–O (C–O–C) stretching). Many sharp peaks in the  $500\text{--}1600\text{ cm}^{-1}$  region weaken even disappeared in the spectra of WGH-Naringin complex micelles. This may be due to the fact that the benzene ring of naringin mainly occupied the hydrophobic cavity of WGHs during the binding process, which indicated that naringin was encapsulated in micelle. In addition, when naringin was incorporated into the micelles, the O–H bands that were originally located at  $3327\text{ cm}^{-1}$  exhibited a certain degree of redshift, confirming the existence of hydrogen bonding between naringin and micelles. Moreover, the shift of the amide I (C–O stretching) also proved the presence of hydrogen bonding during the formation of delivery system (Wang, Wang, Yang, Guo, & Lin, 2015).

### 3.2.3. Intrinsic fluorescence spectra

Fluorescence quenching is a frequent method to characterize the interaction between proteins and small molecules. The addition of small molecules may reduce the fluorescence intensity of complexes, and the binding constant of proteins can be obtained by studying the fluorescence quenching process of protein. The fluorescence intensity gradually decreased with the increase of naringin concentration, indicating the endogenous fluorescence of WGHs was quenched by naringin. And a spectral blueshift of the emission maximum took place, which proved that naringin was combined with aromatic amino acids. The similar results were also found between Great Northern bean protein and curcumin (Zhang, Xie, Feng, Liu, & Luo, 2021).

The Fluorescence quenching method was used to better understand the complexation of naringin with WGHs. The linear function of  $F_0/F$  versus naringin micromolar concentration was shown in Fig. 3, and the  $K_a$  values for WGH-naringin complex micelles at different DH values were calculated to be  $2.36 \times 10^{12}$ ,  $3.31 \times 10^{12}$ ,  $4.0 \times 10^{12}$ ,  $3.50 \times 10^{12}$ ,  $3.46 \times 10^{12}\text{ L}\cdot\text{M}^{-1}\text{ s}^{-1}$  respectively, higher than the maximal dynamic quenching constant ( $2.0 \times 10^{10}\text{ L}\cdot\text{M}^{-1}\text{ s}^{-1}$ ). This revealed that the static quenching occurred to the binding process between the sample and naringin, which was caused by the intermolecular adsorption due to forces such as hydrophobic interactions, rather than fluorescence

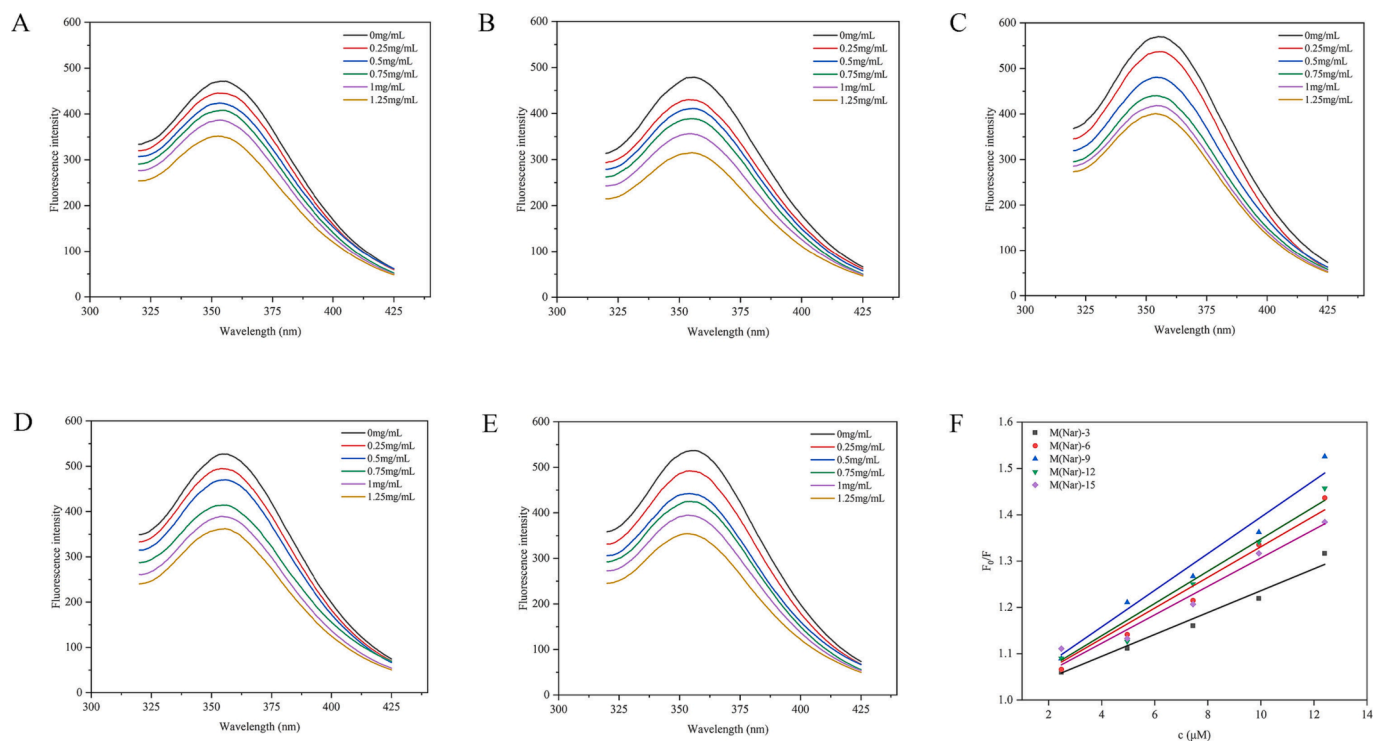


**Fig. 3.** Effect of naringin concentration on the fluorescence intensity of WGHs at different DHs values ranging from (A) 3%; (B) 6%; (C) 9%; (D) 12% to (E) 15%, respectively; (F) Stern-Volmer plots of WGH fluorescence quenching caused by complexing with naringin.

quenching caused by the diffusion and collision of dynamic molecules (Hu et al., 2019). Additionally, the value of the  $K_b$  was used as an indicator of the strength of the binding affinity between WGH and Nar, which was  $0.74 \times 10^4$ ,  $1.01 \times 10^4$ ,  $1.29 \times 10^4$ ,  $1.09 \times 10^4$ ,  $0.91 \times 10^4$  L·M<sup>-1</sup>, respectively.  $K_b$  showed a similar trend to loading capacity encapsulation efficiency, confirming that the load capacity was determined by the affinity between WGH and naringin. The increased binding affinity may be due to the increased degree of hydrolysis, which exposed more binding sites and enhanced the force between WGH and naringin molecules. The degree of hydrolysis did not affect the number of binding sites ( $\approx 1$ ). Enzymatic hydrolysis also contributed to the same impact on the interaction between EGCG and whey protein isolate hydrolysates (Zhao, Lin, Gao, Gong, & Mao, 2022).

### 3.2.4. TEM

TEM can observe the morphology of nano-micelles at the

microscopic level, and Fig. 4 displayed the micromorphology of WGHs and naringin-loaded micelles. More uniform spherical shapes in micelles consisting of hydrolysate (DH  $\leq 12$  %) were noticed, and the size gradually decreased with the increase of DH. This may be because smaller protein fragments were produced with the increase of enzymatic hydrolysis time. When the degree of hydrolysis continued to increase to 15 %, the micelle size increased significantly, and some aggregates appeared in sight, which may be due to that continuous heat induction forced the peptide chains to curl and aggregate. The particle size distribution can also reflect the change in micelle morphology. Two peaks distributed in the range of 0–50 nm and 80–200 nm appeared in all the samples, and with the increase of DH, the distribution peaks shifted to smaller size, indicating a reduction in particle size. The appearance of larger aggregates also resulted in large particle size distribution peaks at 200 nm when DH exceeded 12 %, which was consistent with the result of TEM. Compared with the WGHs, the naringin-loaded micelles had

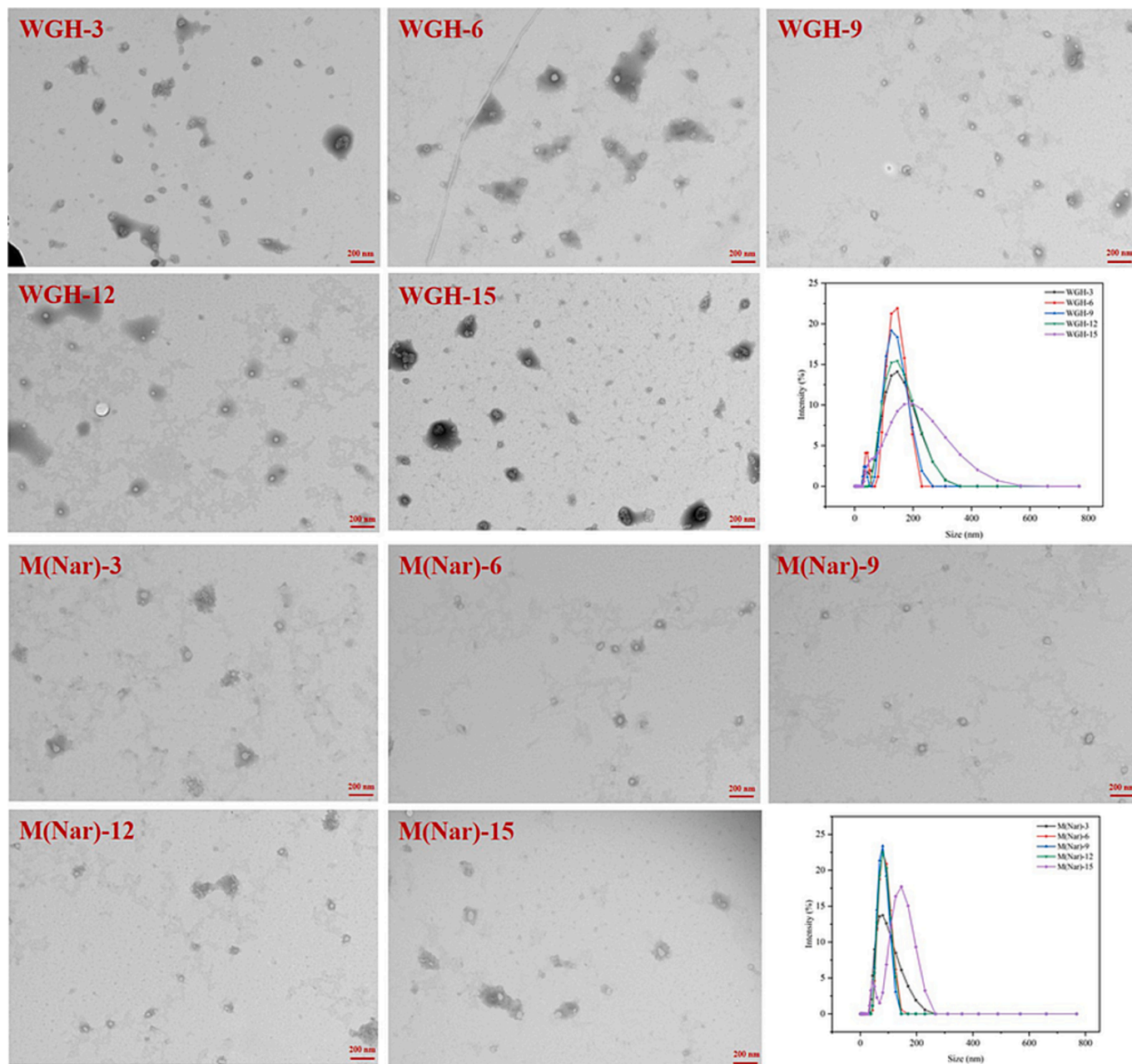


Fig. 4. TEM images and size distributions of WGHs and M(Nar)s with different DHs. Scale bar: 200 nm. Staining technique: negative staining. Magnification: 30,000 $\times$ .

smaller sizes and uniform spherical shapes, and one peak was observed for all the samples. The incorporation of naringin did not influence the morphology of micelles. Du et al. (2019) also found that the morphology of  $\alpha$ -lactalbumin micelles did not change after interacting with  $\beta$ -carotene. The size of micelles observed in TEM images was smaller than that of micelles determined using DLS. This may be attributed to the solvent effect that a hydration layer existed on the surface of the sample in an aqueous solution, and evaporated during the drying process of the observed sample, resulting in a decrease in micelle size (Wang et al., 2013).

### 3.2.5. Stability of nano-micelles

**3.2.5.1. Storage stability.** The storage stability of WGH-Naringin complex micelles was investigated and performed in Fig. 5A. The particle size of micelles prepared by WGHs ( $DH \leq 9\%$ ), especially M(Nar)-9, increased slightly after storage for 12 d. While great changes occurred to the particle size of micelles modified with WGH-15 for the reason that larger particle size and less surface charge led to the instability of the structure. The unstable chemical property of naringin is an important factor limiting its use in food applications. 4.9 % of naringin in the free naringin solution was decomposed. The experimental findings indicated that oxygen did not significantly affect the degradation of naringin. This could be attributed to the fact that the reactivity of flavonoids towards oxygen solely depends on the structure of the central ring. Flavanones and flavanes demonstrate chemical stability when exposed to oxygen, whereas flavones and flavonols are more susceptible (Ioannou, M'Hiri, Chaaban, Boudhrioua, & Ghoul, 2018). Our results corresponded with these observations. Naringin encapsulated in micelles was rarely decomposed as illustrated in Fig. 5B. The protective effect of WGHs on naringin can be attributed to the following points: the loaded naringin was mostly located at the core of micelles, reducing direct contact with the environment. Besides, WGHs contained plentiful hydroxy, carboxyl, and other active groups, which might act as antioxidants to inhibit the oxidation and degradation of naringin. Encapsulation of zein hydrolysate has also been discovered to prevent the degradation of curcumin (Lei et al., 2022).

**3.2.5.2. Photochemical stability.** Naringin is sensitive to ultraviolet light and easily degrades under exposure to UV light. Micelle is an efficient packaging method to protect them from degradation. The degradation curves for different samples were shown in Fig. 5C. Only 45.2 % of the free naringin was reserved after 48 h UV light. The retention rates of naringin encapsulated in micelles were higher than free naringin, and M(Nar)-9 showed better resistance to UV light, which was 78.6 %. It is obvious that the photochemical stability of naringin significantly increased, and the shell formed by the polypeptides obstructed ultraviolet radiation and slowed down the degradation process of naringin.

**3.2.5.3. Heat stability.** Heating treatment is a common processing method in the food industry. As shown in Fig. 5D, the content of naringin decreased after being heated for 180 min, indicating that high temperature could cause damage to the micelle structures. However, the retention rate of naringin remained high at 83.4 %, which proved that WGHs had an excellent encapsulation effect on naringin, preventing it from being exposed to the environment. Jiang et al. (2018) also demonstrated that  $\alpha$ -lactalbumin micelles loaded with Cur and Ant exhibited better thermal stability.

In conclusion, it can be stated that WGHs serve as an efficient carrier to enhance the chemical stability of naringin. The protective effect of WGHs can be credited to the subsequent factors. Typically, oxidation occurs at the surface of the particles, with naringin loaded mostly in the core of the micelles in place of the shell or surface. And the hydrophilic amino acids presented on the exterior of WGHs can be tightly bound to the aqueous environment through hydrogen bonding, forming a

protective barrier against temperature and light. Meanwhile, the micelle structure formed by the WGHs created a physically stable system for the naringin, and therefore naringin did not reconvert from the amorphous to the crystalline form after encapsulation (Wu et al., 2021).

### 3.2.6. In vitro digestion

The insoluble characteristic and unstable chemical properties bring about the low bioavailability and difficult development and utilization of naringin. Nano-micelles are commonly used for the encapsulation and delivery of hydrophobic substances. Therefore, the bioavailability and stability of free naringin and encapsulated naringin were evaluated in the simulated digestion system. It is reported that the absorption of hydrophobic active compounds mainly occurs in the intestine. Naringin released from the nano-micelles was transferred to the bile salt mixed micelles, and the percentage of naringin content in the micellar phase was considered bioavailability (Ye et al., 2023). As shown in Fig. 5E, the bioavailability of free naringin was 10.2 % after digestion of simulated gastric juices, while that of encapsulated naringin was lower than that of free naringin. This may be due to the reason that the shell formed by WGHs prevented the destruction of naringin by enzymes in the stomach environment. He, Wang, Tian, and Zhan (2023) also got the similar conclusion. It can also be found that the protection effect of polypeptides with lower DH was worse, which may be attributed to the fact that the high molecular weight and high hydrophobic polypeptide components had relatively poor stability in stomach digestion (Wang, Xie, & Li, 2019). After 2 h digestion in the intestinal tract, the bioavailability of free Nar was only 17.3 %, indicating that a large number of naringin was not transferred to the bile salt mixed micelles. Compared with free naringin, the bioavailability of naringin encapsulated by WGHs was significantly improved, and the maximum value was 46.8 % (M(Nar)-12). This may be due to the fact that the micelles composed by WGHs increased the solubility of naringin and promoted the micellar process with bile salt. The bioavailability of naringin encapsulated in micellar structure was significantly higher than that of the free state. Several reasons contributed to the occurrence of this phenomenon. Firstly, the encapsulation of WGHs may cause naringin to change from the crystalline form to the amorphous state, which has a higher solubility and bioavailability (Varshosaz, Ghassami, & Ahmadipour, 2018). Secondly, the micelles composed by WGHs had smaller particle sizes, which resulted in a higher specific surface area. This allowed for a quicker release of naringin into the surrounding intestinal fluid. Thirdly, WGHs were easily digested by substances such as pancreatic enzymes and generated more water-soluble peptides, which could bind and solubilize naringin.

Partial digestive fluid was collected to figure out the stability of naringin after the whole simulated digestion (Fig. 5F). Naringin was easily degraded under neutral or alkaline conditions, such as small intestine, and exhibited low chemical stability. The chemical stability of naringin encapsulated by WGHs significantly rises, which may be because WGHs effectively isolated naringin from the water environment of the small intestine, thus inhibiting the degradation and increasing the stability of naringin. These results indicate that hydrolysate can be used as a carrier for the oral administration of naringin.

### 3.3. The relationship between structure and encapsulation performance

The assembly process of micelles load with naringin was shown in Fig. 5G. The enzymatic process of WG generated multiple amphiphilic peptide fragments that were categorized into hydrophilic and hydrophobic regions. Charged and polar amino acids, like glutamine, were predominantly found in the hydrophilic portion, whereas the hydrophobic portion was chiefly composed of amino acids with neutral and nonpolar side chains, such as leucine and isoleucine. The hydrophobic ends of peptides had a tendency to aggregate due to their poor interaction with water molecules, which resulted in a reduction of the surface area exposed to water. More hydrophilic groups were in contact with the

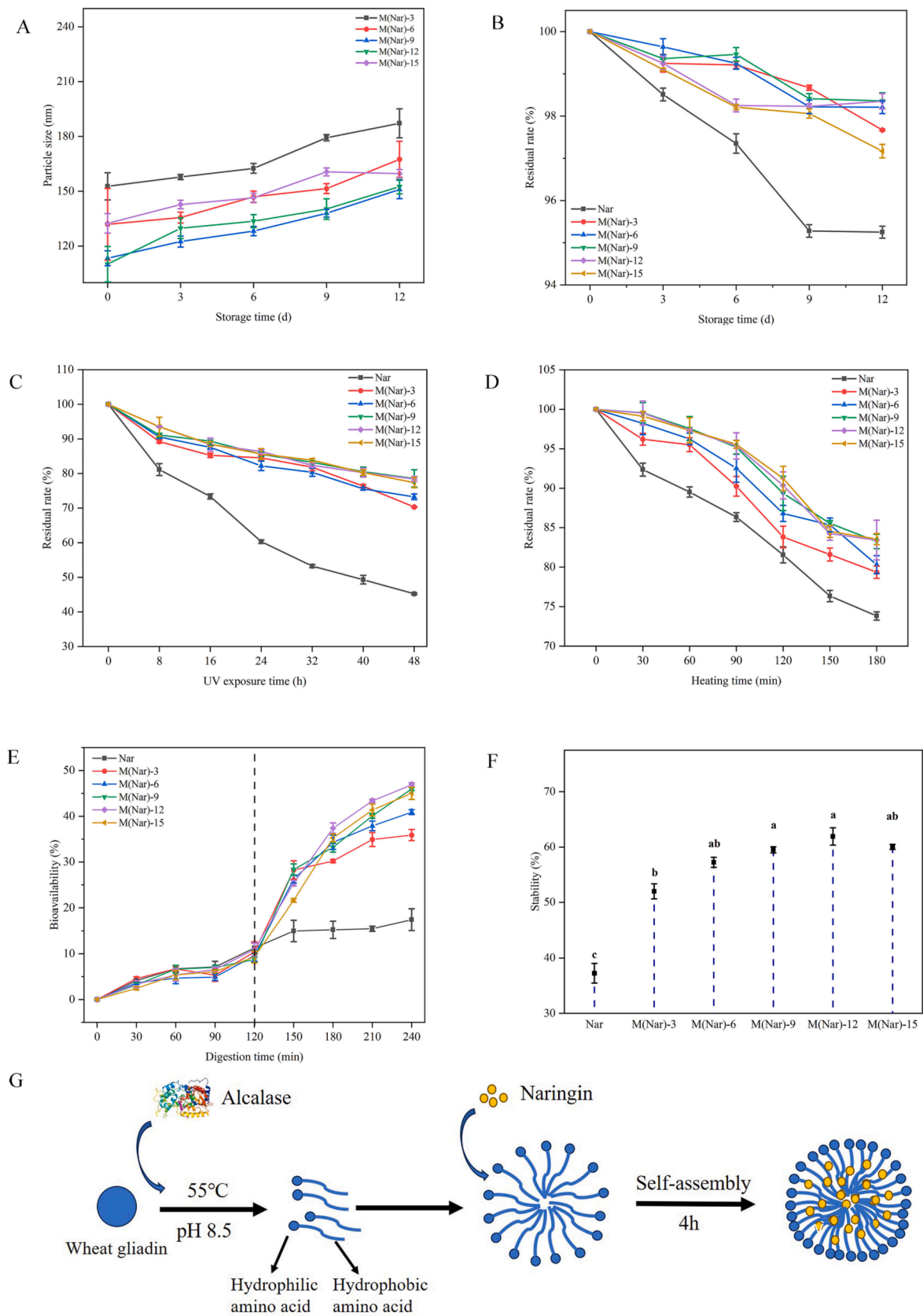


**Fig. 5.** (A) Particle size and (B) Naringin residual rate at different storage time; (C) Naringin residual rate under the exposure of UV light; (D) Naringin concentration in sample solutions during stored at 90 °C for different time; (E) Bioavailability; (F) Stability of naringin in digestion; (G) The illustration of micelles loaded with naringin. Different capital letters (a-c) indicate significant differences ( $P < 0.05$ ).

aqueous environment, and formed hydrogen bonds with water molecule, thereby stabilizing the peptide configuration (Wang, Fu, Hu, & Zhong, 2022). Micelle structures were formed during the assembly process, and the reaction entropy was reduced, resulting in a thermodynamically stable state. When naringin was mixed with WGHs, naringin was able to diffuse into micelles and interact with them. The amide group in the main chain of WGHs, as well as the amino groups in the side chain, can form hydrogen bonds with the hydroxyl group in the structure of naringin. Besides, since the amino acid composition of WGHs was similar to that of WG, which was rich in hydrophobic amino acids such as glutamine/acid and leucine, these hydrophobic groups tended to exhibit high reactivity and interact with the non-polar aromatic ring of naringin, resulting in the encapsulation of naringin within the micelle core to achieve the purpose of encapsulation.

In general, the ability of micelles to encapsulate hydrophobic compounds is influenced by two factors. Firstly, the accessibility of compound into the interior of the micelles, which is mainly predicated on the surface properties of the micelles (Wang & Zhao, 2022). Proteolysis resulted in alterations to the compact protein structure, as inferred by infrared spectroscopy and circular dichroism analyses. The treatment caused disruption of protein hydrogen bonds and hydrophobic interactions, and formed polypeptides with more flexible structure. A decrease in CMC values suggested an enhancement in the interfacial properties of the peptides (Lin, Lai, Chen, & Li, 2016). The flexible structure of WGHs led to a notable increase in contact area and promoted hydrophobic interactions between naringin and hydrolysates. Secondly, the location and strength of the interaction of the bioactive compounds with the protein molecules are also crucial, which is linked to the exposure of hydrophobic residues of the proteins and their structural arrangement within the micelles. The binding sites of WGHs and naringin were exposed during the enzymolysis process. The degree of change in protein structure was affected by DH and had an impact on the character of peptide binding to naringin. Peptides with lower DHs had fewer binding sites and were unable to interact with multiple sites of naringin simultaneously. In contrast, peptides with higher DHs were prone to self-aggregation through hydrophobic interactions, thus reducing the availability of binding sites. The encapsulation properties of WGHs can be modified by adjusting DH, and had an impact on EE. It had been suggested in the literature that an increase in surface hydrophobicity contributed to the encapsulation of hydrophobic substances by peptides, as non-covalent interactions are believed to be mainly induced by hydrophobic interactions (Zhao, Lin, Gao, Gong, & Mao, 2022). In this experiment, the surface hydrophobicity showed a decreasing trend, mainly due to the exposure of hydrophilic groups, which may damage the encapsulation of polypeptides. However, the hydrophilic section of the peptide chain stabilized the peptide arrangement through hydrogen bonding, which enhanced the stability of micelle formation, and in turn, improved EE. Furthermore, the rise in amphipathy and solubility aided in sustaining the dispersion of micelles, and enhanced stability in an aqueous solution. It also helped to improve the biocompatibility of the micelles and was more favorable for exploitation.

#### 4. Conclusions

In this experiment, WGHs with different structural properties were successfully fabricated by controlling the DH of proteolysis, and micelles consisted of peptides and naringin were formed. Alcalase broke the chemical bonds inside the protein, making the structure tend to disorder, and gradually decomposed into amphiphilic polypeptide fragments. The surface hydrophobicity was reduced during this process, while the solubility of the protein in water was significantly increased. CMC was also improved during this process. In addition, peptides produced by enzymatic hydrolysis had the ability to self-assemble, and created an ordered and adjustable structure, which could interact noncovalently with biologically active substances (naringin). The polypeptides formed

a dense protective shell around naringin, which hindered the oxidative decomposition of naringin and improved its bioavailability. Remarkably, WGHs with limited hydrolysis (DH around 12 %) showed superior encapsulation and protection for naringin. The appropriate DH may be a crucial factor in the encapsulation properties, stability and digestibility of micelles. This paper provides a theoretical explanation for the utilization of amphiphilic peptide micelles composed of water-insoluble proteins as a delivery system for hydrophobic bioactive substances.

#### CRediT authorship contribution statement

**Zhiyong Wang:** Investigation, Writing – original draft, Writing – review & editing. **Xiaoyi Cheng:** Conceptualization, Data curation, Methodology. **Fanda Meng:** Conceptualization. **Haotong Guo:** Formal analysis. **Zhengqin Liu:** Supervision, Visualization. **Huan Wang:** Project administration, Visualization. **Jing Xu:** Project administration, Supervision. **Hua Jin:** Project administration, Visualization. **Lianzhou Jiang:** Funding acquisition, Resources.

#### Declaration of competing interest

The authors declare that they have no known competing financial interests or personal relationships that could have appeared to influence the work reported in this paper.

#### Data availability

No data was used for the research described in the article.

#### Acknowledgments

This work was supported by the Key Research and Development projects of Heilongjiang Province [GA21B001], the National Natural Science Foundation of China [No. 31901605], College Student SIPT Innovation Training Program of Heilongjiang Province [S202310224106], and College Student SIPT Innovation Training Program of Northeast Agricultural University [X202310224142].

#### References

- Ai, M., Tang, T., Zhou, L., Ling, Z., Guo, S., & Jiang, A. (2019). Effects of different proteases on the emulsifying capacity, rheological and structure characteristics of preserved egg white hydrolysates. *Food Hydrocolloids*, 87, 933–942.
- Avramenko, N. A., Low, N. H., & Nickerson, M. T. (2013). The effects of limited enzymatic hydrolysis on the physicochemical and emulsifying properties of a lentil protein isolate. *Food Research International*, 51(1), 162–169.
- Barak, S., Mudgil, D., & Khatkar, B. S. (2015). Biochemical and functional properties of wheat gliadins: A review. *Critical Reviews in Food Science and Nutrition*, 55(3), 357–368.
- Chaaban, H., Ioannou, I., Paris, C., Charbonnel, C., & Ghoul, M. (2017). The photostability of flavanones, flavonols and flavones and evolution of their antioxidant activity. *Journal of Photochemistry and Photobiology A-Chemistry*, 336, 131–139.
- Cheng, X., Yang, S., Fang, Q., Dai, S., Peng, X., Sun, M., Lian, Z., Liu, Y., Yang, J., Xu, J., Wang, H., & Jiang, L. (2023). Biomacromolecule assembly of soy glycinin-potato starch complexes: Focus on structure, function, and applications. *Carbohydrate Polymers*, 317, Article 121101.
- Cheng, X., Wang, H., Wang, Z., Zhao, Q., Lou, M., Meng, F., Jin, H., Xu, J., & Jiang, L. (2024). Development and characteristics of emulsion gels with microwave-assisted ferulic acid covalently modified soy protein: Structure, function and digestive properties. *Food Hydrocolloids*, 146, Article 109230.
- Du, Y., Bao, C., Huang, J., Jiang, P., Jiao, L., Ren, F., & Li, Y. (2019). Improved stability, epithelial permeability and cellular antioxidant activity of  $\beta$ -carotene via encapsulation by self-assembled  $\alpha$ -lactalbumin micelles. *Food Chemistry*, 271, 707–714.
- Fathi, M., Donsi, F., & McClements, D. J. (2018). Protein-based delivery systems for the nanoencapsulation of food ingredients. *Comprehensive Reviews in Food Science and Food Safe*, 17(4), 920–936.
- Gómez, A., Gay, C., Tironi, V., & Avanza, M. V. (2021). Structural and antioxidant properties of cowpea protein hydrolysates. *Food Bioscience*, 41, Article 101074.
- He, W., Wang, P., Tian, H., & Zhan, P. (2023). Self-assembled zein hydrolysate glycosylation with dextran for encapsulation and delivery of curcumin. *Food Bioscience*, 51, Article 102364.

- Hu, Y., Bao, C., Li, D., You, L., Du, Y., Liu, B., Li, X., Ren, F., & Li, Y. (2019). The construction of enzymolyzed alpha-lactalbumin based micellar nanoassemblies for encapsulating various kinds of hydrophobic bioactive compounds. *Food Function*, 10(12), 8263–8272.
- Ioannou, I., M'Hiri, N., Chaaban, H., Boudhrioua, N. M., & Ghoul, M. (2018). Effect of the process, temperature, light and oxygen on naringin extraction and the evolution of its antioxidant activity. *International Journal of Food Science and Technology*, 53(12), 2754–2760.
- Jiang, P., Huang, J., Bao, C., Jiao, L., Zhao, H., Du, Y., Fazheng, R., & Li, Y. (2018). Enzymatically partially hydrolyzed  $\alpha$ -Lactalbumin peptides for self-assembled micelle formation and their application for coencapsulation of multiple antioxidants. *Journal of Agricultural and Food Chemistry*, 66(49), 12921–12930.
- Jiang, Z., Sontag-Stroh, T., Salovaara, H., Sibakov, J., Kanerva, P., & Lopenon, J. (2015). Oat protein solubility and emulsion properties improved by enzymatic deamidation. *Journal of Cereal Science*, 64, 126–132.
- Jin, J., Okagu, O. D., Yagoub, A. E. A., & Udenigwe, C. C. (2021). Effects of sonication on the in vitro digestibility and structural properties of buckwheat protein isolates. *Ultrasonics Sonochemistry*, 70, Article 105348.
- Kadam, D., Palamthodi, S., & Lele, S. S. (2019). Complexation of curcumin with *Lepidium sativum* protein hydrolysate as a novel curcumin delivery system. *Food Chemistry*, 298, Article 125091.
- Lei, L., Liang, X. Y., Su, C. R., Nag, A., Yang, X. Q., & Yuan, Y. (2022). The self-assembled zein hydrolysate-curcumin nanocomplex: Improvement on the stability and sustainable release of curcumin. *Journal of the Science of Food and Agriculture*, 102(13), 5729–5737.
- Lin, L., Lai, Y., Chen, K., & Li, C. (2016). Preparation and surface activities of modified soy protein-dextrin surfactants. *Journal of Surfactants and Detergents*, 19(1), 19–28.
- Liu, K., Zha, X., Li, Q., Pan, L., & Luo, J. (2021). Hydrophobic interaction and hydrogen bonding driving the self-assembling of quinoa protein and flavonoids. *Food Hydrocolloids*, 118, Article 106807.
- Majzoobi, M., Abedi, E., Farahnaky, A., & Aminlari, M. (2012). Functional properties of acetylated glutenin and gliadin at varying pH values. *Food Chemistry*, 133(4), 1402–1407.
- Rajib, B., & Ranjini, B. (2013). Encapsulation of hydrophobic drugs in pluronic F127 micelles: Effects of drug hydrophobicity, solution temperature, and pH. *Langmuir*, 29, 4350–4356.
- Ruthvika, J., Yogesh, A., & Sarika, W. (2018). Pharmacokinetic, pharmacodynamic and formulations aspects of naringenin: An update. *Life Sciences*, 215, 43–56.
- Peng, D., Jin, W., Li, J., Xiong, W., Pei, Y., Wang, Y., Li, Y., & Li, B. (2017). Adsorption and distribution of edible gliadin nanoparticles at the air/water interface. *Journal of Agricultural and Food Chemistry*, 65, 2454–2460.
- Qi, P., Wei, Y., Yue, Y., Yan, Z., & Zheng, L. (2006). Biochemical and molecular characterization of gliadins. *Molecular Biology*, 40(5), 713–723.
- Sheng, L., Tang, G., Wang, Q., Zou, J., Ma, M., & Huang, X. (2020). Molecular characteristics and foaming properties of ovalbumin-pullulan conjugates through the Maillard reaction. *Food Hydrocolloids*, 100.
- Stefanovic, A. B., Jovanovic, J. R., Balanc, B. D., Sekuljica, N. Z., Tanaskovic, S. M. J., Dojcinovic, M. B., & Knezevic-Jugovic, Z. D. (2018). Influence of ultrasound probe treatment time and protease type on functional and physicochemical characteristics of egg white protein hydrolysates. *Journal of Poultry Science*, 97(6), 2218–2229.
- Tavano, O. L., Berenguer-Murcia, A., Secundo, F., & Fernandez-Lafuente, R. (2018). Biotechnological applications of proteases in food technology. *Comprehensive Reviews in Food Science and Food Safe*, 17(2), 412–436.
- Varshosaz, J., Ghassami, E., & Ahmadi-pour, S. (2018). Crystal engineering for enhanced solubility and bioavailability of poorly soluble drugs. *Current Pharmaceutical Design*, 24(21), 2473–2496.
- Wang, B., Xie, N., & Li, B. (2019). Influence of peptide characteristics on their stability, intestinal transport, and in vitro bioavailability: A review. *Journal of Food Biochemistry*, 43, Article e12571.
- Wang, C., Fu, L., Hu, Z., & Zhong, Y. (2022). A mini-review on peptide-based self-assemblies and their biological applications. *Nanotechnology*, 33(6), Article 062004.
- Wang, G., Yu, B., Wu, Y., Huang, B., Yuan, Y., & Liu, C. (2013). Controlled preparation and antitumor efficacy of vitamin E TPGS-functionalized PLGA nanoparticles for delivery of paclitaxel. *International Journal of Pharmaceutics*, 446, 24–33.
- Wang, P., Tao, H., Wu, F., Yang, N., Chen, F., Jin, Z., & Xu, X. (2014). Effect of frozen storage on the foaming properties of wheat gliadin. *Food Chemistry*, 164, 44–49.
- Wang, X., & Zhao, Z. (2022). Improved encapsulation capacity of casein micelles with modified structure. *Journal of Food Engineering*, 333.
- Wang, Y., Wang, J., Guo, J., Wan, Z., & Yang, X. (2017). Amphiphilic zein hydrolysate as a delivery vehicle: The role of xanthophylls. *LWT - Food Science and Technology*, 79, 463–470.
- Wang, Y., Wang, J., Yang, X., Guo, J., & Lin, Y. (2015). Amphiphilic zein hydrolysate as a novel nano-delivery vehicle for curcumin. *Food Function*, 6(8), 2636–2645.
- Wu, Z., Zhao, C., Li, R., Ye, F., Zhou, Y., & Zhao, G. (2019). Insights into the micellization of octenylsuccinated oat  $\beta$ -glucan and the uptake and controlled release of  $\beta$ -carotene by the resultant micelles. *Journal of Agricultural and Food Chemistry*, 67(26), 7416–7427.
- Wu, Z., Zhao, C., Huang, Y., Ye, F., & Zhao, G. (2020). Molecular mechanism underlying the effects of temperature and pH on the size and surface charge of octenylsuccinated oat  $\beta$ -glucan aggregates. *Carbohydrate Polymers*, 237, Article 116115.
- Wu, Z., Gao, R., Zhou, G., Huang, Y., Zhao, X., Ye, F., & Zhao, G. (2021). Effect of temperature and pH on the encapsulation and release of  $\beta$ -carotene from octenylsuccinated oat  $\beta$ -glucan micelles. *Carbohydrate Polymers*, 255.
- Yan, S., Wang, Q., Zhang, S., Huang, Y., Zhu, H., Qi, B., & Li, Y. (2024). Oxidized dextran improves the stability and effectively controls the release of curcumin loaded in soybean protein nanocomplexes. *Food Chemistry*, 431.
- Ye, G., Wu, T., Li, Z., Teng, M., Ma, L., Qin, M., Zhao, P., & Fu, Q. (2023). Preparation and characterization of novel composite nanoparticles using zein and hyaluronic acid for efficient delivery of naringenin. *Food Chemistry*, 417, Article 135890.
- Zhao, J., Lin, W., Gao, J., Gong, H., & Mao, X. (2022). Limited hydrolysis as a strategy to improve the non-covalent interaction of epigallocatechin-3-gallate (EGCG) with whey protein isolate near the isoelectric point. *Food Research International*, 161.
- Zhang, Y., Xie, L., Feng, S., Liu, F., & Luo, Y. (2021). Mechanistic study on the nanocomplexation between curcumin and protein hydrolysates from Great Northern bean (*Phaseolus vulgaris* L.) for delivery applications in functional foods. *LWT-Food Science and Technology*, 139, Article 110572.